Quantification of microfluidic dye mixing using front line tracking in curvature scale space

Stephan Jonas*[a,b], Elaine Zhou[c], Brendan Huang[c], Michael A. Choma[b,c,d], Thomas M. Deserno[a]

[a] Department of Medical Informatics, RWTH Aachen University, Pauwelsstr. 30, 52057 Aachen, Germany
[b] Department of Diagnostic Radiology, Yale School of Medicine, 333 Cedar St, New Haven, CT 06520-8042, USA
[c] Department of Biomedical Engineering, Yale School of Engineering and Applied Sciences, 10 Hillhouse Avenue, New Haven, CT 06520–8267, USA
[d] Department of Pediatrics, Yale School of Medicine, 333 Cedar St, New Haven, CT 06520-8042, USA

* sjonas@mi.rwth-aachen.de; phone +49 241 80-88-795; fax +49 241 80-33-88-795; irma-project.org

ABSTRACT

Microfluidic mixing or mixing at low Reynolds number is dominated by viscous forces that prevent turbulent flow. It therefore differs from conventional mixing (e.g., stirring milk into coffee), as it is driven primarily by diffusion. Diffusion is in turn dependent on (i) the concentration gradient along the interface between two fluids (dye front line) and (ii) the extent of the interface itself. Previously, we proposed an in vivo method to microscopically monitor the mixing interface using Shannon information entropy as mixing indicator and explored the use of length of dye front line as an indirect measure of mixing efficiency. In this work, we present a robust image processing chain supporting quantitative measurements. Based on data from ciliated surfaces mixing dye and water, the dye-water interface front line is extracted automatically using the following processing steps: (i) noise reduction (average filtering) and down sampling in time to reduce compression artifacts; (ii) subtraction imaging with key reference frames in RGB color space to remove background; (iii) segmentation of dye based on color saturation in HSV color space; (iv) extraction of front line; (v) curve smoothing in curvature scale space (CSS) with an improved Gaussian filter adaptive to the local concentration gradient; and (vi) extraction of length. Evaluation is based on repeated measurements. Reproducibility in unaltered animals is shown using intra- and inter-animal comparison. Future work will include a more comprehensive evaluation and the application to datasets with multiple classes.

Keywords: Curvature scale space, front line tracking, video microscopy, subtraction imaging, microfluidic mixing

1. INTRODUCTION

Cilia are whip-like organelles that protrude from the surface of certain epithelial cells. Their ability to produce flow plays an important role in many aspects of adult and pediatric health, for example, in reproduction, in developmental biology, in distinct organs such as the embryonic heart or the lungs, where cilia generate flow of mucus out of the respiratory tract. Yet, most work on artificial or biological cilia focus on the efficiency of single cilia but there are no methods available to quantify an integrated readout of the performance of a biological ciliated surface[1]. However, this joint performance has fundamental impact on the efficiency of cilia-generated flow. In prior work, we demonstrated the ability of ciliated surfaces to drive complex flow patterns similar to microfluidic mixers dependent on the geometric boundaries[2]. Thus, we here propose a technique to use the microfluidic mixing performed by a ciliated surface as an integrated readout of ciliary performance. Mixing at low Reynolds number (cilia-scale) is driven only by stirring and diffusion, not by turbulent flow that is present at high Reynolds number, for example when stirring milk into coffee[3,4]. Given that diffusion is dependent on the concentration gradient along the mixing interface, mixing speed increases with larger interfaces. Therefore, the extent of the interface between the two mixing media is a good predictor of mixing

efficiency. The data was acquired with a small animal model, *Xenopus*, whose embryos have a ciliated skin that drives flow[5]. *Xenopus* embryos are immobilized in the center of a circular well, 6 mm in diameter, in a custom-built microfluidic chip, which has 1 mm wide channels to deliver dye (presented at BMES 2012). After delivering a bolus of 1.8 micro liters of dye to the chamber, high definition (HD, Cannon 5D mark II) video microscopy of cilia-driven mixing was acquired over 180 seconds of mixing. All animals were imaged at similar stages (age), so similar mixing efficiency was expected. In addition, reproduction experiments of all animals were made with the same animal performing a cycle of mixing dye and flushing repeatedly within a short period of time.

2. METHOD

Quantitative measurements require robust image processing. The huge data volume of microscopic video sequences must be processed automatically without any user interaction. This requires adaptive algorithms that are robust to noise, blur, defocus and illumination changes. Previously, we proposed an in vivo method to microscopically monitor the mixing interface using Shannon information entropy as mixing indicator[6]. The processing presented in this work however extracts the length of front line between dye and water mixed in a microfluidic setting with known geometric configuration[7]. A sample set with unaltered animals was generated based on an acquisition protocol accounting for issues with data used in prior versions of this work.
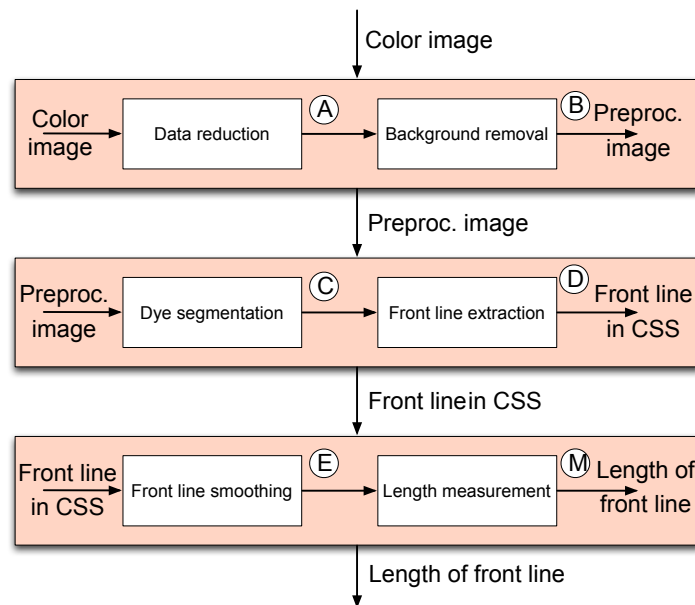

Fig. 1: Image processing chain divided into the three main steps: image preprocessing (top), front line extraction (middle), and postprocessing and extraction of length in front line. Circled letters refer to panels in Fig. 2.

2.1 Image processing

Since the magnification during acquisition was not fixed (170-200 pixel/mm), all sizes were normalized to millimeter during post processing. Image processing of the new data chains five steps (Fig. 1, 2)[8]:

1.   Data reduction: MPEG4 (avc1 codec) compression artifacts are removed applying a moving average filter over time to the movies. Since HD videos (1920×1080 p, 29.9 fps) generate about 180 MB data per second, the video stream is down-sampled in time resulting in six frames per second. In addition, the video is spatially binned with a window of 2 ×2 pixels. This removes noise and reduces the amount of data to be handled (final video dimensions: 960 × 540 p, ~6 fps).

2. Background removal: The image background is removed by subtracting a key reference frame that was acquired before the start of the experiment from all subsequent images. Subtraction is performed in RGB color space, each channel is subtracted individually from its counterpart in the reference image.

3. Dye segmentation: The dataset was generated with an acquisition protocol that included a stable light source and fixed background color. Therefore, the dye is segmented from the background subtraction data using fixed thresholds in the saturation channel of the HSV color space.

4. Front line extraction: The front line is extracted by tracing the outline of the segmented dye and converting it into curvature scale space[9].

5. Front line smoothing: To account for minor errors in segmentation, the extracted front line is smoothed in CSS at a low scale with a Gaussian filter with 25 pixel in size independently in the x and y dimension. To incorporate the physical information of the concentration gradient along the front line, the Gaussian filter is weighted by the gradient in saturation at each position within a 3×3 kernel.

6. Length measurement: The length of front line is calculated on the resulting smoothed outline by integrating the length of all measurement points along the front line.

Visual inspection of 20 analyzed acquisition showed that the front line was tracked adequately throughout initial mixing of dye but became less stable the more diluted the dye became. This is due to very low gradients along the dye front line, the front line becomes too fuzzy to be defined adequately. Since our assumptions on the mixing efficiency rely on a front line with high concentration gradient, we will focus our analysis on the time of initial mixing during which a high gradient concentration is still present. This is possible since diffusion of dye, even along an interface with a high gradient, is a much slower process than active stirring.
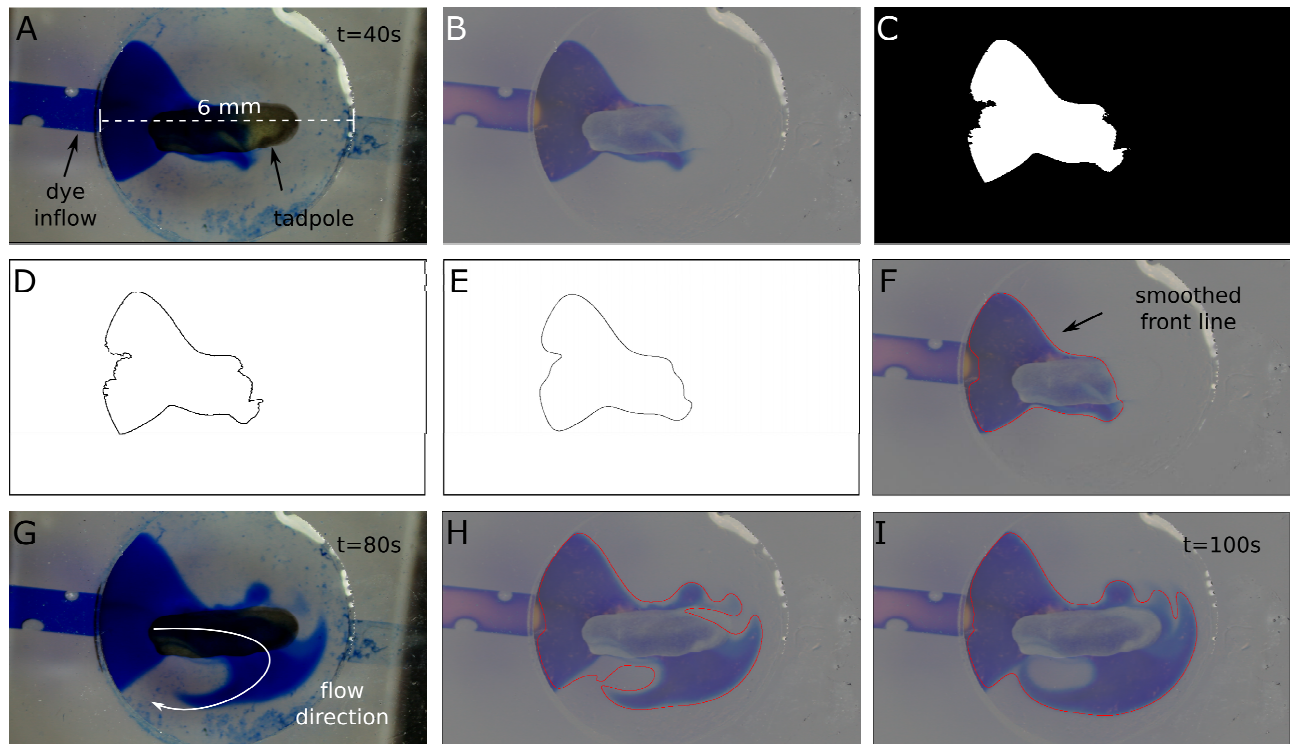

Fig. 2: Visualization of image processing chain for example animal 8. (A) Original image at 40 seconds of mixing; (B) key-frame subtracted image; (C) segmentation of dye; (D) dye front line as represented in CSS; (E) smoothed dye front line; (F) overlay of dye front line onto angiography image; (G) original image at 80 seconds of mixing; (H) corresponding overlay of dye front line onto angiography image at 80 seconds of mixing; (I) example of dye backfolding and overlay of resulting shorter front line. Compare Fig. 3
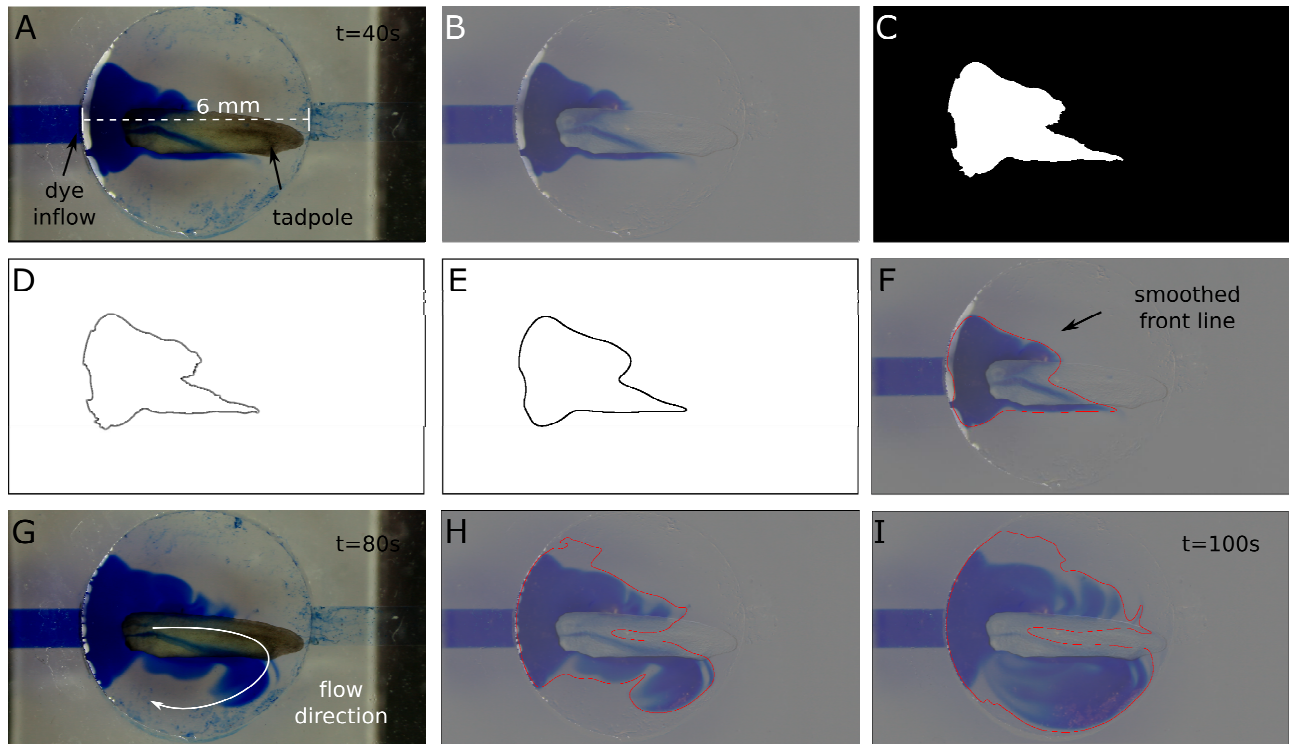
Fig. 3: Visualization of image processing chain for example animal 2 with different mixing. (A) Original image at 40 seconds of mixing; (B) key-frame subtracted image; (C) segmentation of dye; (D) dye front line as represented in CSS; (E) smoothed dye front line; (F) overlay of dye front line onto angiography image; (G) original image at 80 seconds of mixing; (H) corresponding overlay of dye front line onto angiography image at 80 seconds of mixing; (I) example of dye backfolding and overlay of resulting shorter front line. Compare Fig. 2.

Visualization of the processing showed the contribution of each image processing step (Fig. 2). The key frame subtraction from the original image (Fig. 2/3.A) completely removed the background and animal from the image (Fig. 2/3.B). Thresholding of saturation yields a segmentation that represents the dye in the original image (Fig. 2/3.C) and the outline is traced and converted into CSS (Fig. 2/3.D), where it is smoothed to remove segmentation errors and to increase robustness (Fig. 2/3.E,F). Frames of time points during increased mixing show the backfolding of the dye into itself (Fig. 2/3.G-H). This effect is also represented by abrupt changes in the visualization of length of front line as a function of time (Fig. 2/3.I). The complete image processing was performed at a speed of about 3 frames per second, resulting in an overall computing time of approximately 20 minutes per acquisition.

2.2 Intra-animal repeatability

For an initial evaluation of our method, we used intra-animal reproduction. For this, repeated acquisitions of a single unimpaired embryo mixing dye were made. A total number of five repetitions were performed. Due to the chemical properties of the dye used in the experiments, the embryo however ceased to generate flow. For comparison reasons, only the first two acquisitions are compared and the variance is computed between the length of front line of the first and second acquisition for each point in time during the first 60 seconds (Fig 4.A).

2.3 Inter-animal repeatability

To further investigate the reproducibility of our measurement, we created a second dataset (n=8) with single acquisitions of multiple animals mixing dye to evaluate the feasibility of our method towards comparing ciliary mixing within one class (Fig. 4.B).
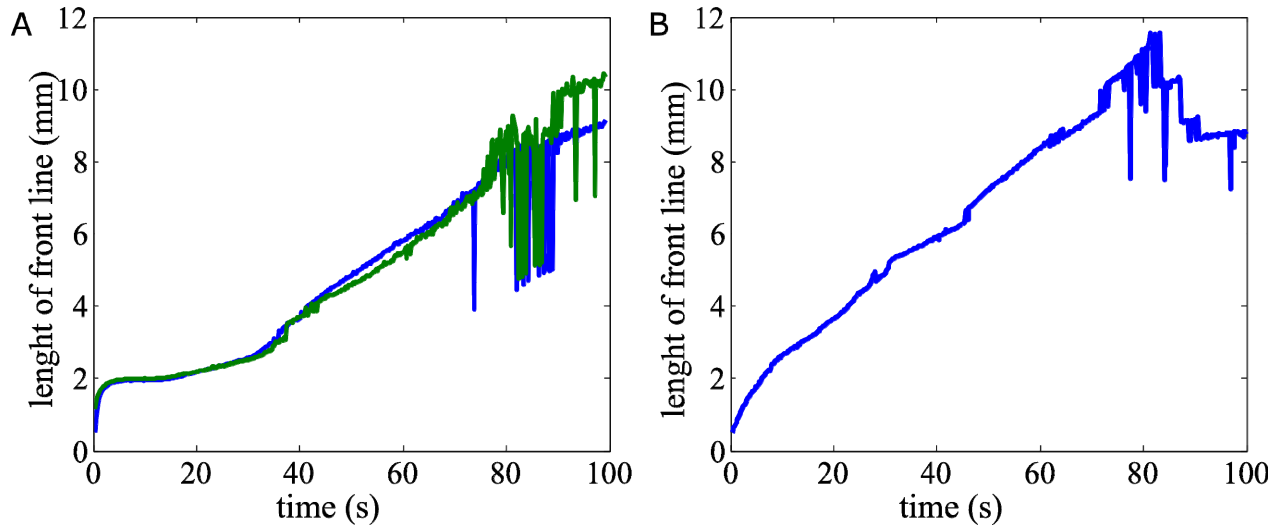
Fig. 4: Length of front line plotted as a function of time for intra-animal repeatability of a younger animal (A) and the length of front line of the animal in Fig. 2.

3. RESULTS

The repeatability experiments of our intra-animal repeatability experiment showed that the same animal had similar development in length of front line (*stdev* = *.15* mm, within first 60 seconds) upon repeated delivery of dye (Fig. 4.A). The feasibility experiment using acquisitions across multiple animals at the same stage showed that all animals in the dataset had an average length of front line of 9.35 mm (stdev = 1.54 mm) after one minute of mixing (Fig. 4.B, Table 1.).

4. DISCUSSION

The reported visual inspection shows that the length of front line is extracted correctly and can be used as a measurement of mixing with some restrictions based on the physical properties of the mixing process. The limiting factor observed during visual inspection is the fact that the length of front line abruptly decreases once the mixing pattern folds back into itself forming a ring. This happens since we only measure the length of the outermost front line to prevent segmentation

Table 1: Length of front line for inter-animal repeatability experiments

Animal	LFL 30 sec (mm)	LFL 60 sec (mm)	Time of first backfolding (s)
1	6.75	11.63	65
2	8.07	11.61	95
3	8.12	9.10	not observed
4	4.23	7.07	85
5	7.91	8.64	not observed
6	6.93	9.02	not observed
7	7.98	9.03	80
8	7.85	8.75	90
Mean	7.23	9.35	
STD	1.32	1.54	

errors resulting into holes from interfering with our result. The backfolding effect was observed after 90 seconds of mixing time with the given geometric configuration (Table 1, Fig. 2.E, time 80-100 s). Thus, our processing focuses on the first minute of mixing and extracts the length of front line after this timeframe unless prior folding is observed.

The quantitative analysis of the length of front line shows that the measurement has low variance in length between different reproduction acquisitions of the same animal at a given point in time. This indicates that their mixing efficiency is similar which is congruent with visual inspection and is expected of animals within the same stage. Thus, our image processing is sound can robustly extract the length of front line for repeated measures. However, experiments with younger animals have shown, that the dye used in the experiments itself can have an effect on the animal as it's chemical properties can lead to a change in osmotic pressure which in turn leads to a bloating of the animal.

In addition, our analysis was applied to acquisitions of different animals at the same stage and the length of front line was extracted. A slightly elevated variance was observed in comparison to the repeated measures, which can be attributed to slightly different age of the animals. Comparisons with prior results showed that age has a significant impact on the ability to drive flow.

5. CONCLUSION

In conclusion, our method is a reproducible measurement under the given image acquisition protocol. This indicates that the front line is a suitable indirect indicator of mixing performance. Further improvements of our method will include a change in the imaging protocol towards an osmotic neutral dye as well as optimization of the geometric configuration to prevent early backfolding. Since mixing patterns might play a specific role for mixing efficiency, a comparison of mixing patterns based on CSS is also possible[10]. Additionally, future work will focus on extending this framework to include active contours for smoothing during post processing and the application of this analysis towards biological problems, especially in the evaluation of severeness of respiratory diseases.

REFERENCES

[1] Parrilla, E., Armengot, M., Mata, M., Cortijo, J., Riera, J., Hueso, J.L., and Moratal, D., "Optical flow method in phase-contrast microscopy images for the diagnosis of primary ciliary dyskinesia through measurement of ciliary beat frequency," Proc. ISBI, 1655 – 1658 (2012)

[2] Jonas, S., Bhattacharya, D., Khokha, M. and Choma, M.A., "Microfluidic characterization of cilia-driven fluid flow using optical coherence tomography-based particle tracking velocimetry," BOE, 2(7), 2022-2034 (2011).

[3] Squires, T.M., Quake, S.R., "Microfluidics: Fluid physics at the nanoliter scale," Reviews of Modern Physics, 77(3), 977-1026 (2005).

[4] Dusenbery, D.B., [Living at Micro Scale: The Unexpected Physics of Being Small], Harvard University Press, Cambridge, pp448 (2009)

[5] Werner, M.E. and Mitchell, B.J., "Understanding ciliated epithelia: The power of Xenopus," GENESIS, 50(3), 176-185 (2012).

[6] Chandrasekera, K., Jonas, S., Bhattacharya, D., Khokha, M. and Choma, M.A., "Entropy-based measures of in vivo cilia-driven microfluidic mixing derived from quantitative optical imaging," Proc. SPIE 8207, 82073K (2011).

[7] Khatavkar, V.V., Anderson, P.D., den Toonder, J.M.J. and Han Meijer, E.H., „Active micromixer based on artificial cilia," Phys. Fluids, 19(8), 083605- 083618 (2007).

[8] Jonas, S., Deniz, E., Khokha, M.K., Deserno, T.M. and Choma, M.A., „Microfluidic phenotyping of cilia-driven mixing for the assessment of respiratory diseases," Proc. BVM, 135-140 (2012).

[9] Bebis, G., Papadourakis, G., Orphanoudakis, S, "Recognition Using Curvature Scale Space and Artificial Neural Networks," Proc. IASTED SIP (1998).

[10] Abbasi, S., Mokhtarian, F., Kittler, J., "Curvature scale space image in shape similarity retrieval," Multimedia Systems, 7(6), 467–76 (1999).